Application of the Polarimetric Matched Image Filter to the Assessment of SAR Data from the Mississippi Flood Region

J. G. Teti, Jr.†, F. J. Ilsemann†, J. S. Verdi, W.-M. Boerner‡ and S. K. Krasznay

Naval Air Warfare Center
Aircraft Division
Warminster, PA 18974-0591

†JJM Systems, Inc.
One Ivybrook Blvd., Suite 190
Ivyland, PA 18974-1700

‡University of Illinois at Chicago, EECS
Communications, Sensing & Navigation Lab, M/C 154
Chicago, IL 60607-7018

Abstract - The optimal use of polarimetric scattering information provided by multiband synthetic aperture radar (SAR) is examined for its utility to improve the assessment of damage caused by the Mississippi flood of 1993. This natural flood disaster submerged or saturated large geographical regions including extensive farmland, and deposited large amounts of sandy sediment. A polarimetric matched image filter technique based on eigenanalysis is applied to enhance image contrast in selected regions for improved detection and classification of flooded regions. A subset of L-Band SAR data is first radiometrically and polarimetrically calibrated, and then coarsely segmented for the extraction of spatial statistics useful for filter application. The polarimetric matched image filter is applied to increase the contrast between dry and flooded land regions that may include stressed embankments (dikes) and levees, while also reducing speckle. The processing procedure is described, and the potential utility of the results is examined. The results are compared to the span image and verified with ground truth information.

Introduction

The geographically extensive damage caused by many types of natural disasters has established a need for the use of airborne and space sensors to aid in timely damage assessment. The Navy P-3 Polarimetric SAR aircraft [1], and similarly the NASA-JPL Polarimetric AIR-SAR [3], are extremely capable all-weather airborne sensors well suited for natural disaster damage assessment. The recent Mississippi flood of 1993 has provided a fortuitous opportunity to investigate the potential utility of polarimetric SAR imagery [1-5] for the identification of flooded geographical regions that include farmland. Communications with local authorities [6] indicate that farmland damage assessment activities are still actively underway (over one year after the disaster) and are likely to continue for quite some time before completion. Informal discussions between Navy P-3 SAR Program personnel and individuals conducting damage assessment have concluded that aerial observation and associated microwave imagery during the entire duration of the disaster would be extremely helpful for both expedient and successful completion of their efforts. Useful optical imagery has either not been made available or does not exist. Note that optical imagery is not likely to simultaneously provide adequate geographical coverage and useful land feature resolution [4,7], especially for all-weather day/night situations. Radiometrically calibrated conventional SAR imagery provides both large geographical coverage and high resolution suitable for ground truth correlation [4]. However, conventional SAR imagery is difficult to interpret by untrained personnel, and depending upon system polarization characteristics many image features can be masked and undetectable [4,7]. Fully polarimetric SAR imagery provides the capability to utilize polarization matching rather than suffer from polarization mismatch [5,7-10]. The characteristic polarization states of the flooded and dry regions allow their distinction to be enhanced and more completely identified with the use of the polarimetric matched image filter [4,5,7].

SAR polarimetry is based on the concept that characteristic polarization states can be associated with electromagnetic scattering from different surfaces [4,7]. Polarimetric SAR system measurements after radiometric and polarimetric calibration provide estimates of the scattering matrices associated with each image pixel [3,11]. The scattering matrix estimate associated with a particular geographical feature (or terrain type) can be improved by averaging over statistically homogeneous regions within the image that contain the same geographical information (e.g. water or land). Because of the P-3 Systems' high resolution, averaging is performed over relatively small regions of the image to yield very good scattering matrix estimates. Once scattering matrices have been obtained for the appropriate geographical features, eigenanalysis is used on the corresponding Graves and Kennaugh power matrices to synthesize a polarimetric matched filter (PMF) image that maximizes the contrast between the features [5,10]. The resulting PMF image provides enhanced detection and distinction of image features while decreasing speckle. The speckle reduction arises from polarization mismatch introduced by the filter [5].

This paper describes the application of the PMF to a subset of L-Band SAR data collected from the Mississippi flood region. The data is first radiometrically and polarimetrically calibrated, and the corresponding span image is formed. The calibrated polarimetric component images are coarsely segmented to extract both water and land spatial statistics and estimate the associated scattering matrices. The Graves power matrices are formed from the estimated scattering matrices and the PMF is applied. The PMF image result is compared to the span image [2,3,5,7] and verified with ground truth information. Contour representations of the two images are also provided to illustrate the sharp partitioning that is a consequence of the contrast enhancement provided by the PMF [5]. The subsequent sections describe an overview of the SAR radiometric and polarimetric image calibration procedures, polarimetric matched filtering, processed SAR imagery, and conclusions regarding the utility of the PMF for natural disaster damage assessment.

Polarimetric SAR Image Calibration

Polarimetric SAR image calibration involves radiometric and polarimetric compensation. The radiometric procedures basically consist of range attenuation correction, antenna elevation pattern correction, system gain normalization and radar cross section (RCS) calibration. In addition, slant range projection normalization may also be desired. The polarimetric procedures basically consist of phase corrections applied after radiometric calibration [3,11]. The subsequent paragraphs describe an overview of the calibration procedures used on the L-Band Mississippi flood region imagery prior to application of the PMF.

The range attenuation correction follows directly from the radar range equation [3,4] given by

$$P_r = P_t G(\theta,\varphi)\left(\frac{\lambda}{4\pi R}\right)^2 \frac{4\pi\sigma(\theta,\varphi)}{\lambda^2}\left(\frac{\lambda}{4\pi R}\right)^2 G(\theta,\varphi) \qquad (1)$$

where P_r is the received peak power, P_t is the transmitted peak power, G is the one way antenna gain, λ is the radar operating wavelength, σ is the nominal RCS of the range azimuth cell, R is the slant range to the range-azimuth cell, and $(\theta,\varphi)=(az.,el.)$. After the synthetic aperture is formed the total received power is improved by the integration factor $(CR)(PRF)T$ where CR is the pulse compression ratio for down range resolution, PRF is the radar pulse repetition frequency and T is the time duration of the synthetic aperture formation. Using the SAR azimuth resolution given by $\delta_{az} = R\lambda/(2vT)$, (1) can be modified to yield the classical R^{-3}

0-7803-1497-2/94 $4.00 © 1994 IEEE

IEEE Geoscience and Remote Sensing Symposium, 1994. IGARSS '94. 'Surface and Atmospheric Remote Sensing: Technologies, Data Analysis and Interpretation'., International , Volume: 3 , 8-12 Aug 1994. Page(s): 1368 -1370 vol.3

dependency where the implicit SAR processing improvement factor introduced assumes that the range curvature effect has not yet been corrected. However, the basic SAR processor used with data collected by the Navy P-3 SAR system (developed by the Environmental Research Institute of Michigan (ERIM)) accounts for range curvature [1,11]. Consequently, post image formation processing range attenuation correction uses the relation

$$P_r = \frac{P_t G^2 \lambda^2 \sigma}{(4\pi)^3 R^4}(CR)\frac{(PRF)R\lambda}{2v\delta_{az}}\gamma R \qquad (2)$$

where γ accounts for windowing function effects and the angular dependencies of the antenna pattern and RCS have been suppressed. Using (2) the R^{-2} dependency of the range attenuation is removed, and then the system gain factors and angular dependency of the antenna beam in elevation are removed using measured system gain information and antenna gain patterns $G(\theta,\varphi)$. At this stage the SAR image has been *relatively* calibrated and absolute calibration can not be performed unless a known RCS target exists in the scene. For the assessment of natural disaster sites absolute calibration is not felt to play a significant role. The final step in the calibration procedure prior to the application of the PMF involves the phase correction between the polarimetric channels. Without polarimetric calibration targets deployed in the scene, data dependent methods must be utilized. The polarimetric calibration task is to relate the actual scattering matrix S (per pixel) to the measured scattering matrix M. Recall that the scattering matrix [8,9] relates the incident $\bar{E}_i$ and scattered $\bar{E}_s$ electric fields by

$$\begin{bmatrix} E_{sH} \\ E_{sV} \end{bmatrix} = \begin{bmatrix} S_{HH} & S_{HV} \\ S_{VH} & S_{VV} \end{bmatrix} \begin{bmatrix} E_{iH} \\ E_{iV} \end{bmatrix} \qquad (3)$$

where the subscripts indicate horizontal (H) and vertical (V) polarization. The measured scattering matrix M [4] can be related to the actual scattering matrix S by

$$M = R^{\dagger} S T + N \qquad (4)$$

where R and T represent the receive (Rx) and transmit (Tx) imbalance and leakage, and N represents channel noise. The R, T and N matrices are unique for a particular system. The system channel imbalance and leakage characteristics are a consequence of the directional combination of the Tx/Rx and H/V isolation. The Navy P-3 system has sufficient isolation for the subject application requiring (4) to account for only the phase difference between Tx ϕ_t and Rx ϕ_r on the H and V channels. From reciprocity, $\arg(S_{HV}S_{VH}^*) = 0$. Thus, the difference between the transmit and receive phase can be obtained from

$$\langle \arg(M_{HV}M_{VH}^*) \rangle = \phi_t - \phi_r \qquad (5)$$

where the average operation can be performed over the entire image field. In practice, it is customary to set $M_{HV} = M_{VH}^*$. Exploiting the information contained in the measured like-polarized data leads to

$$\langle \arg(M_{HH}M_{VV}^*) \rangle = \langle \arg(S_{HH}S_{VV}^*) \rangle + \phi_t + \phi_r \qquad (6)$$

where the average operation must be taken over a carefully chosen region of the image field. Unlike (5), computing (6) is sensitive because it is scene (RCS) dependent. In addition, to find the phase quantities of interest in (6), a particular region in the image that corresponds to single bounce scattering should be chosen to ensure that $\langle \arg(S_{HH}S_{VV}^*) \rangle = 0$ [2,12]. Using an appropriate region of the image, the pulse interleaving characteristics of the Navy P-3 Polarimetric SAR system operation must be taken into account to evaluate (6) [1,11]. The results presented here do not use (6). After phase calibration the measured scattering matrix M is equated to S, and the basis-invariant span image is computed by [2,4,5]

$$P_{span} = \left\{ |S_{HH}|^2 + |S_{VV}|^2 + 2|S_{HV}|^2 \right\}. \qquad (7)$$

Polarimetric Matched Filtering

To define the PMF [4,5,10], let the polarization state of the transmitted or incident wave be expressed as

$$\bar{E}_i = \left(E_{iH}(x,y)\hat{e}_x + E_{iV}(x,y)\hat{e}_y \right) e^{j(2\pi ft \pm kz)} \qquad (8)$$

where the widely accepted definitions for notation apply. The horizontal and vertical components of the incident electric field are given by

$$\begin{bmatrix} E_{iH} \\ E_{iV} \end{bmatrix} = \begin{bmatrix} a_H \cos(\alpha) \\ a_V \sin(\alpha) e^{j\beta} \end{bmatrix} \qquad (9)$$

where the angles α and β are related to the orientation ψ and ellipticity χ angles by

$$\begin{aligned} \cos(2\alpha) &= \cos(2\psi)\cos(2\chi), \\ \tan(\beta) &= \tan(2\chi) / \sin(2\psi). \end{aligned} \qquad (10)$$

The scattered electric field is given by (4). The energy density (power) in the scattered field is given by

$$P_s = \bar{E}_s^{\dagger}\bar{E}_s = \bar{E}_i^{\dagger} S^{\dagger} S \bar{E}_i = \bar{E}_i^{\dagger} G \bar{E}_i \qquad (11)$$

where $G = S^{\dagger}S$ is the Hermitian Graves power matrix. Consider two different regions in an image denoted by A and B, where it desirable to enhance the detection of A in the presence of B. Note that A could represent an object to be detected and B could represent clutter. The associated scattering matrices can be used with (11) to match the polarization state of the incident field to maximize the power in the scattered field. The quantity to maximize is given by [5,10]

$$\Omega = \frac{P_s^A}{P_s^B} = \frac{\bar{E}_i^{\dagger} G_A \bar{E}_i}{\bar{E}_i^{\dagger} G_B \bar{E}_i}. \qquad (12)$$

Maximizing Ω reduces to solving the generalized eigenvalue problem [13]

$$G_A \bar{E}_i^{opt} = \lambda G_B \bar{E}_i^{opt}. \qquad (13)$$

Note that $G_B = I$, the identity matrix, is a special case. The quantity $0 \le (\lambda_1 - \lambda_2)/(\lambda_1 + \lambda_2) \le 1$ indicates the separation extremes that can be observed between the characteristic polarization signatures of A and B. The optimum polarization state $\bar{E}_i^{opt}$ is given by the eigenvector corresponding to the largest eigenvalue λ_1. The PMF image results from

$$P_s^{opt} = \bar{E}_i^{opt\dagger} G_S \bar{E}_i^{opt} \qquad (15)$$

where G_S is the Graves power matrix for each pixel of the calibrated image. Note that more elaborate "Optimal Polarimetric Contrast Enhancement Coefficients (OPCEC)" are derived in [9], and their utility is demonstrated in [4,5,7].

Processed SAR Imagery and Conclusions

This section presents the calibrated L-Band SAR span and PMF images to allow direct comparison. In addition, contour maps of the images are provided to highlight edge characteristics of the images. The L-Band SAR span image is shown in Figure 1, and the PMF image is shown in Figure 2. The PMF result enhances the distinction of the flooded regions allowing the full extent of the potential crop and property damage to be more easily identified. Figures 3 and 4 show the corresponding contour maps of the images, and clearly highlight the edge enhancement performance of the PMF image. Communications with local authorities [6] have verified the extent of the flooded regions identified by the PMF SAR image.

Related research activities are currently being conducted with POL-SAR interferometric imagery constructed with large temporal baselines to detect subsurface deformations. The large temporal baseline interferograms require data that is collected from time delayed overflights of identical geographical regions. The details of this work will be reported separately [14].

IEEE Geoscience and Remote Sensing Symposium, 1994. IGARSS '94. 'Surface and Atmospheric Remote Sensing: Technologies, Data Analysis and Interpretation'., International , Volume: 3 , 8-12 Aug 1994. Page(s): 1368 -1370 vol.3

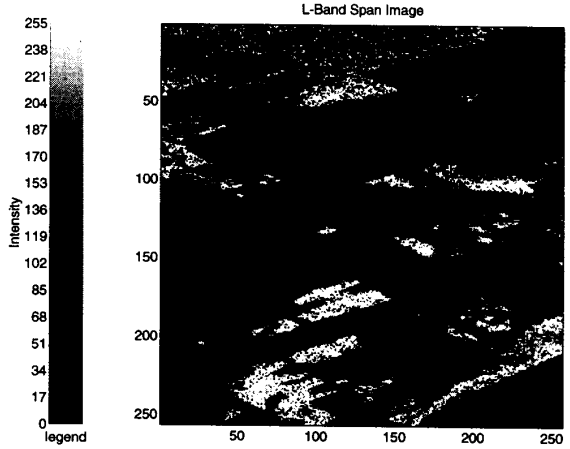

Figure 1: L-Band SAR span image.

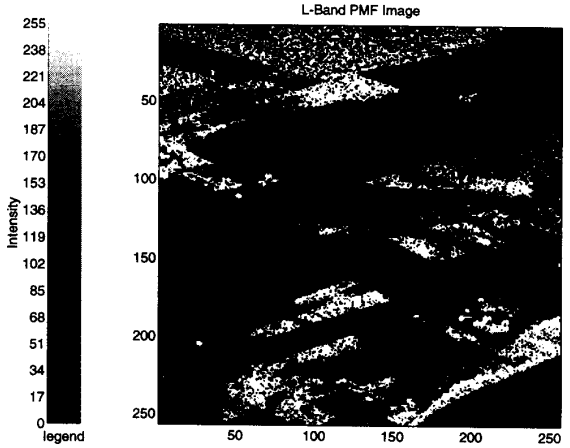

Figure 2: L-Band SAR PMF image.

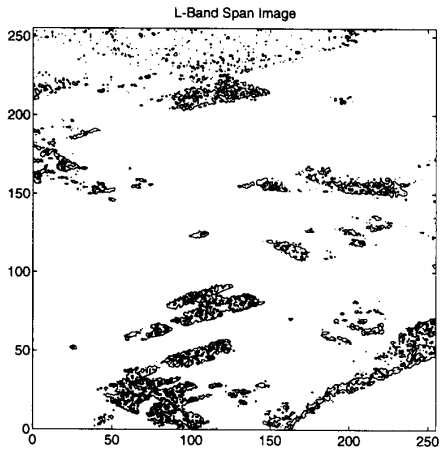

Figure 3: Contour map for the L-Band SAR span image.

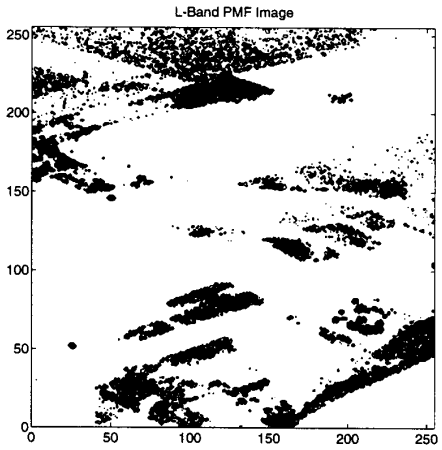

Figure 4: Contour map for the L-Band SAR PMF image.

References

[1] R. Sullivan, A. Nichols, R. Rawson, C. Haney, F. Darreff and J. Schanne, Jr., "Polarimetric X/L/C-Band SAR," *Proc. of the IEEE National Radar Conference*, pp. 9-14, 1998.

[2] W.-M. Boerner, B.-Y. Foo and H.-J. Eom, "Interpretation of the Co-Polarization Phase Term $(\phi_{HH} - \phi_{VV})$ in High Resolution SAR Imaging Using the JPL CV-990 Polarimetric L-Band SAR Data," *IEEE Trans. on Geoscience and Remote Sensing*, vol. 25, no. 1, pp. 72-82, Jan. 1987.

[3] J. J. van Zyl, H. A. Zebker and C. Elachi, "Imaging Radar Polarization Signatures: Theory and Observation," *Radio Science*, vol. 22, no. 4, pp. 529-543, July-Aug. 1987.

[4] W.-M. Boerner, et al (eds), *Proc. of the NATO-Advanced Research Workshop on Direct and Inverse Methods in Radar Polarimetry*, 18-24 Sept. 1988, Proceedings, (1,938 pages), NATO-ASI Series C: Math and Physics Sciences, Vol. C-350, Parts 1&2, Kluwer Academic, Dordrecht, NL, 1992.

[5] W.-M. Boerner, M. Walther and A. Segal, "The Concept of the Polarimetric Matched Signal and Image Filters: Application to Radar Target Versus Clutter Optimal Discrimination in Microwave Imaging and Sensing," *Int'l Journal on Advances in Remote Sensing*, (EAReL), Boulogne-Billancourt, France, vol. 2, no. 1-1, pp. 219-252, Jan. 1993.

[6] Private Communications: Richard Horman, University of Missouri Extension Center, 260 Brown Road, St. Peters, Missouri 63376.

[7] H. Mott and W.-M. Boerner, (eds), *Proc. of SPIE '92 Workshop on Radar Polarimetry*, vol. 1748, Feb. 1993.

[8] W.-M. Boerner, W.-L. Yan, A.-Q. Xi and Y. Yamaguchi, "On the Basic Principles of Radar Polarimetry: the Target Characteristic Polarization State Theory of Kennaugh, Huynen's Polarization Fork concept, and its extension to the Partially Polarized Case," *Proc. of the IEEE*, vol. 79, no. 10, pp. 1538-1550, Oct. 1991.

[9] W.-M. Boerner, C.-L. Liu and X. Zhang, "Comparison of the Optimization Procedures for the 2x2 Sinclair and 4x4 Mueller Matrices in Coherent Polarimetry and Its Application to Radar Target Versus Background Clutter Discrimination in Microwave Sensing and Imaging," *Int'l Journal on Advances in Remote Sensing*, (EAReL), Boulogne-Billancourt, France, vol. 2, no. 1-1, pp. 55-82, Jan. 1993.

[10] A. B. Kostinski B. D. James and W.-M. Boerner, "Polarimetric Matched Filter for Coherent Imaging," *Can. J. Physics*, vol. 66, no. 10, pp. 871-877, Oct. 1988.

[11] D. R. Sheen, A. Freeman and E. S. Kasischke, "Phase Calibration of Polarimetric Radar Images," *IEEE Trans. on Geoscience and Remote Sensing*, vol. 27, no. 6, pp. 719-731, Nov. 1989.

[12] H. J. Eom and W.-M. Boerner, "Statistical Properties of the Phase Difference Between Two Orthogonally Polarized SAR Signals," *IEEE Trans. on Geoscience and Remote Sensing*, vol. 29, no. 1, pp. 182-184, Jan. 1991.

[13] R. Courant and D. Hilbert, *Methods of Mathematical Physics*, Vol. I, Wiley, Inc., New York 1953.

[14] W.-M. Boerner, J. Verdi, J. Dea, P. Hansen, J. van Zyl, E. Rignot and G. Peltzer, "Mapping Lithospheric Stress Displacement in Surface Deformation and Crustal Motion by Repeat Track Space-SAR Interferometry - An Assessment of the State of the Art in Classical Versus Unconventional Earthquake Prediction," *PIERS*, 11-15 July, 1994.

IEEE Geoscience and Remote Sensing Symposium, 1994. IGARSS '94. 'Surface and Atmospheric Remote Sensing: Technologies, Data Analysis and Interpretation'., International , Volume: 3 , 8-12 Aug 1994. Page(s): 1368 -1370 vol.3